Magic Pairs and Structural Transitions in Binary Metallic Clusters

Liviu-Cristian Cune

Department of Theoretical Physics, National Institute for Physics and Nuclear Engineering, PO Box MG-6, RO-077125 Magurele-Bucharest, Romania
Fax: (+40)214575332
E-mail: cune@theory.nipne.ro

Abstract

Structures and binding energies for bimetallic clusters consisting of a large variety of atomic species are obtained for all atomic sizes $N \leq 40$ and all concentrations, using an interatomic potential derived within a quasi-classical description. We find that increasing the difference between the two types of atoms leads to a gradual disappearance of the well-known homo-atomic geometric magic numbers and the appearance of magic pairs corresponding to the number of atoms of each atomic species in binary nanostructures with higher stability. This change is accompanied by structural transitions and ground-state↔isomer inversions, induced by changes in composition or concentration. We find a clear tendency towards phase separation, the core-shell radial segregation being predominant (energetically favored) in this model.

Keywords: Bond theory, Molecular modeling, Nanotechnology, Computational chemistry, Phase transitions

1 Introduction

Experimental and theoretical results show that alloying atomic clusters can lead to new nano-materials with new properties and new functionalities.[1] Therefore, there is a need of detailed studies of such binary clusters, covering a wide range of atomic species. Since the computational effort limits the use of the ab-initio methods to selected compounds, guessed structures or imposed symmetries, so far such extensive studies have been performed using semi-empirical potentials, usually Lennard-Jones potentials (see for example Ref.[2]). Unfortunately, these potentials apply primary to rare-gas compounds, and it is known that bimetallic nanostructures, with their magnetic, optic or catalytic properties, are better candidates for new technological functionalities. Studies using semi-empirical potentials specific to metals, like second-moment approximation to tight-binding potentials, including Gupta[3, 4] and Sutton-Chen[5] potentials, are focused on specific cluster sizes and compositions, occasionally for various concentrations. (See for example Refs. [6, 7, 8, 9, 10, 11, 12]). Sometimes, the structures obtained with these semi-empirical potentials are locally re-optimized using density functional theory (DFT) methods.[6, 7, 8] Here, we present a more general approach, similar in some respect to the one presented in Ref.[2] for binary Lennard-Jones clusters. Using a genuine metallic potential derived and applied previously to homo-atomic clusters,[13, 14] we search for the ground state structures for all binary clusters of size less than 40 and for any concentration; moreover, by varying the coupling constants in a range which covers a large number of metallic elements we try to map out the behavior of the bimetallic clusters in the compositional space. The theory employed in deriving these potentials has been applied also to homo-atomic clusters deposited on surfaces,[14, 15] or to the metallic core of an iron-hydrocarbon cluster.[16] We could add also that the theory provides valuable information when applied to macroscopic object like metallic surfaces, infinite plates or slabs. It provides, for example, a theoretical derivation for the well known Smoluchowski ansatz[17] for the electron density at a metallic surface.[14, 15] The theory applies straightforwardly to hetero-metallic compounds, the simplest case of free binary clusters being reported here.

2 Theory

Using a quasi-classical description for the electrons participating in a metallic bonding, it has been shown that the atomic interactions in a nanostructure can be described by an effective potential[13]

$$\Phi_{ij} = -\frac{1}{2} q z_i^* z_j^* \left(1 - \frac{2}{qR_{ij}}\right) e^{-qR_{ij}} \quad , \tag{1}$$

where R_{ij} are the interatomic distances, q is a variational screening wavevector and z_i^* are the effective ionic charges which depends on the atomic species.[1] It is worth mentioning here that long time ago a similar potential

[1] Atomic units are used: the Bohr radius $a_H = \hbar^2/me^2 \cong 0.53$Å for distances and $e^2/a_H \cong 27.2$eV for energies; $-e$ is the electron charge, m is the electron mass and $\hbar$ denotes the Planck constant.

has been suggested on semi-empirical grounds, with some success, for the H_2 molecule.[18] These effective charges which play the role of coupling constants in the effective atomic interaction (1) can be estimated within the atomic screening theory. They acquire small values, as required by a quasi-classical description.[13] We have, for example, $z^*_{Na} = 0.443$ for sodium, $z^*_{Ba} = 0.339$ for barium and $z^*_{Fe} = 0.579$ for iron. The screening wavevector minimizes the quasi-classical energy, and has a $\bar{z}^{*1/3}$-dependence, where $\bar{z}^*$ is a mean effective charge. This equilibrium value for q leads to a $\bar{z}^{*7/3}$-behavior for the quasi-classical energy. The equilibrium structures are obtained by minimizing the total potential energy, $\sum_{i<j} \Phi_{ij}$, and depend on q only as a scale factor for the atomic positions. In addition, for homo-atomic clusters the interatomic distances depends on effective ionic charges only through q, giving rise to universal geometric forms.[13] For binary clusters, the equilibrium structures depends also on the ratio between the effective charges of the two atomic types leading to more stable geometric forms (core-shell clusters), distorted homo-atomic forms or even new structures with new symmetries. On the other hand, the binding energy depends on the values of both effective valence charges; it is obtained by minimizing the quasi-classical energy[13]

$$E_q = \frac{27\pi^2}{640} q^4 \sum_{i=1}^{N} z_i^* - \frac{3}{4} q \sum_{i=1}^{N} z_i^{*2} + \frac{1}{2} \sum_{i \neq j=1}^{N} \Phi_{ij} \quad , \tag{2}$$

with respect to the variational screening wavevector q, and by adding the exchange energy $E_{ex} = -(9/32)q^2 \sum_i z_i^*$. In equation (2) the first term is the kinetic energy of the electrons moving in the self-consistent Hartree field

$$\varphi = \sum_i z_i^* \exp(-q\,|\mathbf{r} - \mathbf{R}_i|)/\,|\mathbf{r} - \mathbf{R}_i| \quad , \tag{3}$$

where $\mathbf{R}_i$ are the atomic positions, and having the electron density $n = q^2\varphi/4\pi$. We may note that the self-consistent field (3) is a superposition of screened Coulomb potentials. The second term in equation (2) plays the role of an electron self-energy and the last term is the total potential energy. This potential energy include the electron-electron and electron-ion interactions (through the self-consistent field given by equation (3)) and the interaction between positively charged ionic cores.

It is worth emphasizing that the effective potential given by equation (1) is a genuine many-body potential because the variational screening wavevector q, as obtained from the minimum condition $\partial E_q/\partial q = 0$ for the quasi-classical energy (2), has an implicit dependence on all the atomic positions $\mathbf{R}_i$. On the other hand, in the numerical problem of finding equilibrium cluster structures we can avoid the difficult task of minimizing an energy composed of multiparticle potentials by minimizing first a reduced total potential energy, $E_{pot}/q = \sum_{i<j} \Phi_{ij}/q$ with respect to the scaled positions $\mathbf{X}_i = q\mathbf{R}_i$; expressed with these scaled positions, the corresponding scaled potential for (1) has a true two-body form, $\Phi_{ij}/q = -(1/2)z_i^* z_j^* (1 - 2/X_{ij})\exp(-X_{ij})$. In this step we find the equilibrium form in the $X-$space, by finding the equilibrium scaled positions $\mathbf{X}_i^0$. Using the minimum value for the reduced potential energy we minimize the quasi-classical energy (2) and obtain the equilibrium screening wavevector q_0. With this value we obtain the equilibrium positions as $\mathbf{R}_i^0 = \mathbf{X}_i^0/q_0$.

3 Binary clusters

The theory outlined above has been applied to binary clusters $A_n B_{N-n}$, with $N = \overline{2,40}$, $n = \overline{0,N}$ and the ratio $1 \leq z_A^*/z_B^* \leq 2.5$ (step 0.1) of the effective valence charges of the two elements A and B. These parameters cover a very large domain of binary metallic compounds. The minimization of the potential energy has been performed by usual gradient method starting from random initial positions. Using a large number of trials for each cluster increases the chance of finding the true ground-state. The use of large statistical ensembles is required by the increasing number of isomers compared with the homo-atomic case; each isomer, clusters with the same composition and size but with different structure and greater energy compared to the ground-state, is accompanied by the so called homotops, clusters which, up to permutations between different type of atoms, share approximately the same geometric structure and energy. A way to overcome this difficulty is to make such permutations during the minimization of the potential energy, provided they are energetically favorable. Because other authors use the word composition with other meaning it is important to specify that we use the term concentration for the ratio between the number of atoms A and the total number of atoms and composition for the ratio z_A^*/z_B^*. With this conventions, a changed concentration means that some atoms A are replaced by atoms of type B (or vice versa) and a changed compositions means that all the atoms of one type (say A for example) are replaced by atoms of another type (say C for example) and this change is reflected in a variation of the ratio z_A^*/z_B^*; we must note that we can modify the composition by replacing both types of atoms with a new pair of atoms, but usually we will keep the B atoms unchanged in the following discussion because all the qualitative results are independent of the absolute value of z_B^*. By taking permutations during the minimization of the potential energy we keep the concentration and composition constant, so we will find a

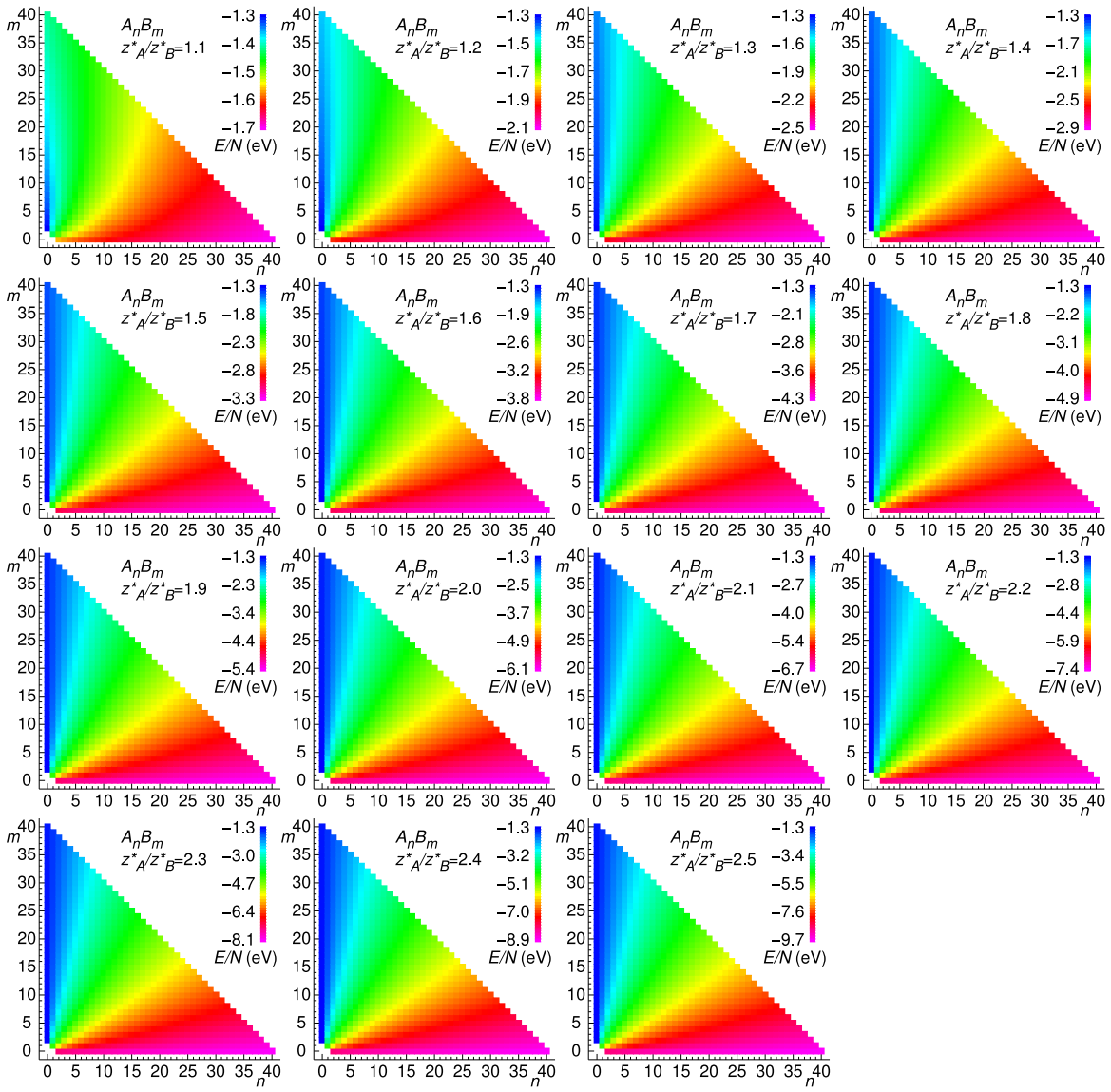

Figure 1: Ground-state energy per atom for binary clusters A_nB_m with $z_B^* = 0.3$

putative global minimum for each cluster size N, concentration n/N and composition z_A^*/z_B^* (*i.e.* 11700 global minima, excepting the homo-atomic global minima). In Refs[2] and [19] the concentration is allowed to change during minimization which reduces drastically the search space at the expense of loosing all the information about a large number of clusters. The results reported here have been obtained using up to 1000 initial random positions for each cluster size, composition an concentration. Finally, the results have been refined by making adiabatic evolutions, *i.e.* starting from each ground-state and the first isomer and going in small (adiabatic) steps toward clusters with different coupling constant z_A^*/z_B^*. The number of ground-states modified by this adiabatic search is less than 0.7%, which gives confidence in the accuracy of the results. For each composition, the binding energies (ground state and isomers) and equilibrium structures have been obtained. The ground-state binding energies per atom for various values of the ratio z_A^*/z_B^* are presented in Figure 1. As stated above, the binding energy depends on both values z_A^* and z_B^*; the energies presented in Figure 1 correspond to $z_B^* = 0.3$ but can be easily scaled to different values of z_B^*; for z_A^*/z_B^* =constant, we can obtain from (2) the following scaling relations for the binding energy E, the screening wavevector q, and the equilibrium positions $\boldsymbol{R}_i$,

$$\begin{aligned} E &= z_B^{*7/3} E_0 + \frac{9}{32} Z_0^* q_0^2 (z_B^{*7/3} - z_B^{*5/3}) \ , \\ q &= q_0 z_B^{*1/3} \ , \\ \boldsymbol{R}_i &= \boldsymbol{R}_i^0 z_B^{*-1/3} \ , \end{aligned} \tag{4}$$

where $Z_0^* = \sum_i z_i^*$ is the total ionic charge; the variables labeled by $'0'$ refer to $z_B^* = 1$. We can see in Figure 1 how the energy range increases at higher z_A^*/z_B^* values; we obtain, for instance, a range of less than 0.5eV for $z_A^*/z_B^* = 1.1$ and more than 8eV for $z_A^*/z_B^* = 2.5$. This energy range variation can be understand as a

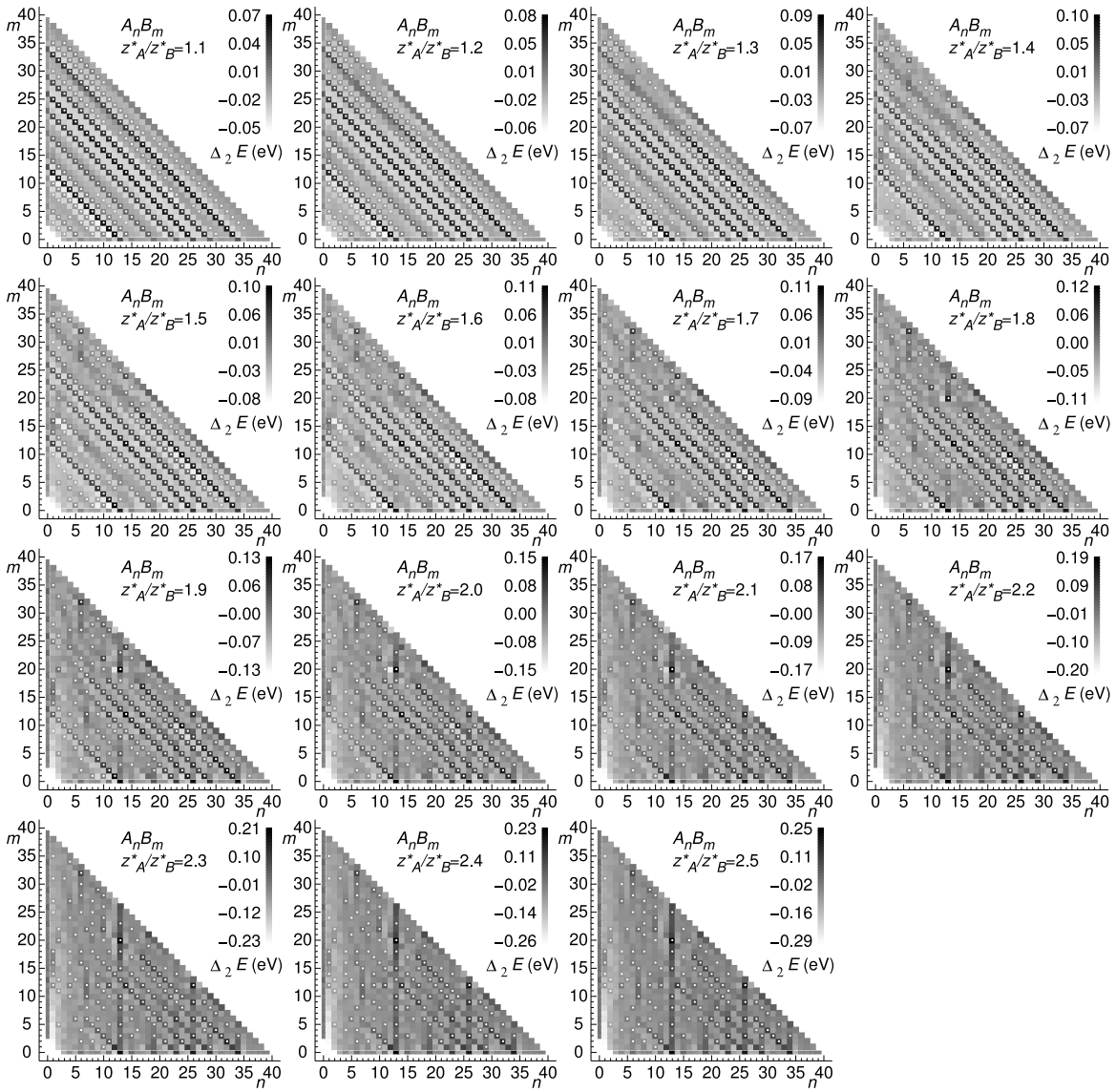

Figure 2: Stability spectrum for various values of z_A^*/z_B^*.

rapid change in the mean effective valence charge $\bar{z}^*$ when we change the concentration for clusters composed of very dissimilar atoms (large z_A^*/z_B^*); as noted above the quasi-classical energy behave like $\bar{z}^{*7/3}$. We may see in Figure 1 that even for large z_A^*/z_B^* the energy is slowly varying for constant concentrations (constant concentration curves are the lines starting from the origin on the graphs shown in Figure 1).

For homo-atomic clusters the stability with respect to the variation of the number of atoms is tested by the second difference of the energy;[20, 21, 22] it defines the so called stability spectrum, sometimes well correlated with the experimental mass-abundance spectrum; its maxima indicate the magic numbers, clusters with higher stability compared to their neighbors. The magic numbers obtained for homo-atomic metallic clusters are 6, 13, 19, 23, 26, 29, 34, ... ;[13] these numbers, now known as geometrical magic numbers, because they are given by the close packing in the icosahedral structures, have been obtained with various other methods like, for example with Morse potentials.[23] For binary clusters we can define two families of such spectra for each type of atoms:

$$\begin{aligned} \Delta_2^A E &= E_{n+1,m} + E_{n-1,m} - 2E_{n,m} \\ \Delta_2^B E &= E_{n,m+1} + E_{n,m-1} - 2E_{n,m} \end{aligned} \tag{5}$$

where $E_{n,m}$ is the ground-state energy of the binary cluster A_nB_m, $\Delta_2^A E$ and $\Delta_2^B E$ indicate the cluster stability with respect to the variation of the number of A-atoms (or B-atoms respectively) at fixed number of B-atoms (or A-atoms respectively). Each spectrum has magic numbers; the coincidence of a maximum in both spectra define a magic pair $\{n, m\}$, *i.e.* a double magic clusters A_nB_m, which indicate the higher stability of the cluster compared to his neighbors: $A_{n-1}B_m$, $A_{n+1}B_m$, A_nB_{m-1} and A_nB_{m+1}. The maxima in a sum spectrum defined

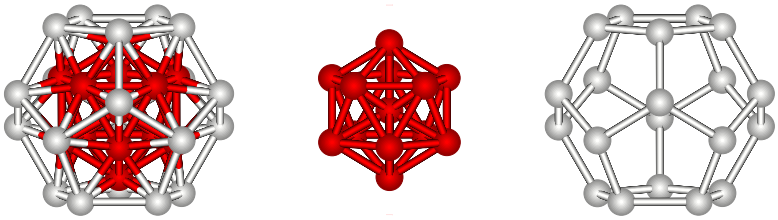

Figure 3: The cluster $A_{13}B_{20}$ (*left*), double magic for $z_A^*/z_B^* \geq 1.7$ and ground-state for $z_A^*/z_B^* \geq 1.6$, displaying an A_{13} icosahedron core (*center*) and a B_{20} dodecahedron shell (*right*).

as

$$\begin{aligned} \Delta_2 E &= \Delta_2^A E + \Delta_2^B E = \\ &= E_{n+1,m} + E_{n,m+1} + E_{n-1,m} + E_{n,m-1} - 4E_{n,m} \end{aligned} \tag{6}$$

can also be viewed as magic pairs; by analogy with the homo-atomic case,[13] we can define a relative abundance $D = \ln I_{n,m}^4 / I_{n+1,m} I_{n-1,m} I_{n,m+1} I_{n,m-1}$, where $I_{n,m}$ is the Boltzmann statistical weight; up to a constant we have $D \simeq \Delta_2 E$, where $\Delta_2 E$ is given by equation (6). The first definition for these magic pairs, viewed as maxima in both relations given in equation (5), is more restrictive; nevertheless, we have found a very close similarity between the results obtained with these two definitions in the whole range of effective valence charges we have studied. The definitions given here for magic pairs follows closely the definition for magic numbers in homo-atomic clusters, which reflects an enhanced stability relative to all the neighbors with one atom more or one atom less. The only differences are that every binary cluster is indexed with two numbers (the numbers of atoms of each species) and has four neighbors instead of two, relative to which we must test the stability. The definition of magic spectra reflect also the condensation and evaporation processes that take place in a majority of experimental setups. Only the first order processes (involving loosing or acquiring of a single atom) are taken into account. It is somehow tempting to consider also, for example, the cluster $A_{n-1}B_{m+1}$ as a neighbor of A_nB_m in the stability spectrum; but A_nB_m can evolve into $A_{n-1}B_{m+1}$ or vice versa only through second order processes (losing an atom of one type and acquiring an atom of another type). Stability relative to such neighbors can be tested by defining a spectrum at fixed size and variable concentration.[1, 9, 24] Also, the mixing energy defined as $\Delta_N = E_{n,m} - (nE_{N,0} + mE_{0,N})/N$, was previously used for describing the relative stability and mixing in binary clusters.[7, 25]

The sum spectrum given by equation (6) is shown in Figure 2 for all the values of z_A^*/z_B^*; the darker squares indicate magic pairs; also, the magic pairs according to the first definition are marked with white dots; we can see the above mentioned similarity between the two definitions. We can see in Figure 2 that for small values of the ratio z_A^*/z_B^* the magic pairs correspond to the homo-atomic magic numbers for $N = n + m$. Once the discrepancy between atomic species increases, this homo-atomic behavior gradually disappears giving place to new magic pairs. This can be explained by the small distortions in the icosahedral symmetry caused by the small difference in the interatomic interactions $A-A$, $A-B$, $B-B$, and by structural transitions to fcc or disordered geometries. The magic pairs are confined to certain regions in the range of the parameter z_A^*/z_B^*. Varying the composition, the magic peaks gradually appear, starting with some value z_A^*/z_B^* and may vanish at a higher z_A^*/z_B^* value. We obtained, for instance, the magic pairs {6,32} for $z_A^*/z_B^* \geq 1.4$, {10,22} for $1.5 \leq z_A^*/z_B^* \leq 2.4$, {13,20} for $z_A^*/z_B^* \geq 1.7$, {14,24} for $1.4 \leq z_A^*/z_B^* \leq 2.0$ and {26,12} for $z_A^*/z_B^* \geq 1.8$, which correspond to clusters having N=32, 33 or 38 which are not homo-atomic magic numbers.[13]

In the lowest range of the z_A^*/z_B^* values the equilibrium structures have with preponderance icosahedral symmetry and display a core-shell atomic arrangement, with the 'heavier', *i.e.* greater effective charge, A-atoms in the center and a B-atoms shell. There is experimental and theoretical evidence for this radial segregation in binary clusters (see for example Refs. [6, 28, 29, 30, 31]). In our model segregation is favored over mixing because the strength of the $A-B$ interaction is always smaller than the $A-A$ interaction (in fact, for a constant interatomic distance and screening wavevector, the strength of the $A-B$ interaction is a geometric mean between the $A-A$ and the $B-B$ interaction; therefore the mixing energy[7, 25] tends to acquire positive values which points out the preference for segregation over mixing in our model; we obtain negative mixing energies for binary clusters with similar type of atoms, $z_A^*/z_B^* \leq 1.3$, at various concentrations, where alloying is favored according to this criterion). The A atoms segregate in the center where atoms have greater coordination numbers and an increasing number of $A-A$ bonds is energetically favorable. The mixing could take place if $A-B$ had been the strongest interaction.[1] Comparing the effective valence charges for various types of atoms we obtain, for example, that the core positions are occupied by Cu atoms in $Ag-Cu$, $Au-Cu$, by Co atoms in $Co-Pt$, $Co-Pd$, by Pd atoms in $Ag-Pd$, $Au-Pd$ and by Pt or Ni atoms in $Pd-Pt$, $Ag-Pt$ or $Ag-Ni$ clusters, in good agreement with other calculations.[6, 9, 12, 25, 26, 27] On the other hand for $Ag-Au$

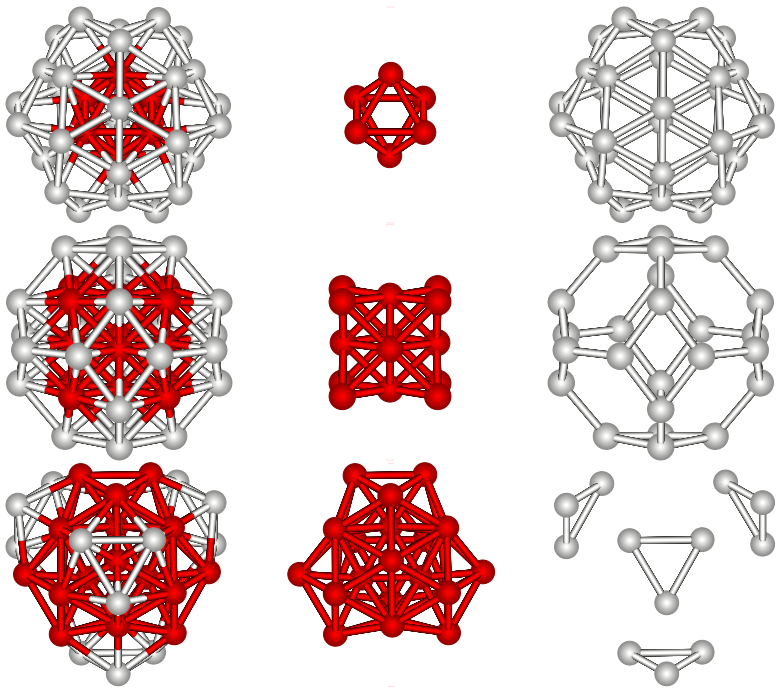

Figure 4: The bimetallic 38-atoms cluster corresponding to the magic pairs {6,32} (the top row), {14,24} (the middle row) and {26,12} (the bottom row).

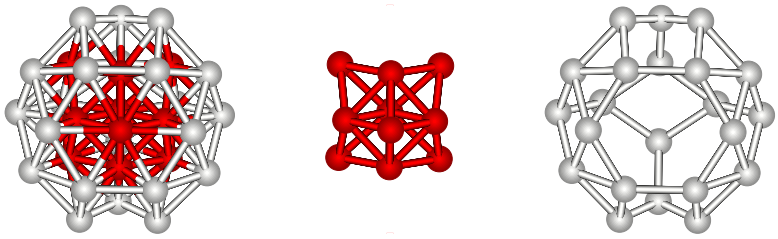

Figure 5: The double magic cluster $A_{10}B_{22}$ (*left*) with a fcc $A-$core (*center*) and an outside $B-$shell (*right*).

systems we obtain that the Ag atoms occupy core positions in contrast to the tendency (although diminished compared to other compounds) towards surface segregation found in Ref. [27] but in agreement with more recent DFT calculations.[25] Although new structures and symmetries appear, the icosahedral symmetry is often obtained for larger values of the ratio of the effective charges of the two atomic species. For example, the magic cluster $A_{13}B_{20}$, whose structure is presented in Figure 3, has a perfect icosahedral symmetry and a core-shell atomic arrangement with a core icosahedron formed by the A-atoms and an outside shell of B-atoms grouped in a perfect dodecahedron. The high stability of this cluster can be explained by the favorable ratio of the numbers of atoms A and B (favorable concentration). The A_{13}-icosahedron core is also magic in the homo-atomic series. In spite of different strengths in the inter-atomic interaction, each atom species occupies distinct icosahedral shells, which do not lead to symmetry distortions, and gives stability. Moreover, the strength of the inter-atomic interaction $A-B$, greater than the $B-B$ interaction, equilibrates the incomplete outside shell (the so called anti-Mackay shell which becomes complete at $N=45$) by maximizing the numbers of $A-B$ bounds in detriment of the weaker $B-B$ bounds. Once the ratio between the two effective charges is decreased this geometric arrangement becomes energetically unfavorable, the homo-atomic ground-state having a rather disordered structure. This is a first example of structural transition induced by composition. Such core-magic structures (the core is magic itself, as a homo-atomic cluster) which are also stable against the variation of the number of B atoms, forming in this way magic pairs, have been obtained, usually for higher z_A^*/z_B^* values, for various magic numbers of A-atoms. For instance, we can identify the magic pairs $\{6,32\}$, $\{13,20\}$, $\{23,m\}$, whit $m=3$, 6 and $\{26,m\}$, with $m=3$, 6, 9, 12.

A particular cluster is the 38-atoms clusters which becomes highly stable, in different equilibrium structures, for the magic pairs $\{6,32\}$, $\{14,24\}$ and $\{26,12\}$. The equilibrium geometric forms for these clusters are shown in Figure 4. The clusters A_6B_{32} and $A_{26}B_{12}$ belong to the above mentioned core-magic structures. The structure $A_{14}B_{24}$ has a fcc symmetry, his A_{14}-core being a face centered cube and the outside B_{24}-shell a truncated octahedron. This is not the only cluster with fcc symmetry obtained by the present approach. The cluster

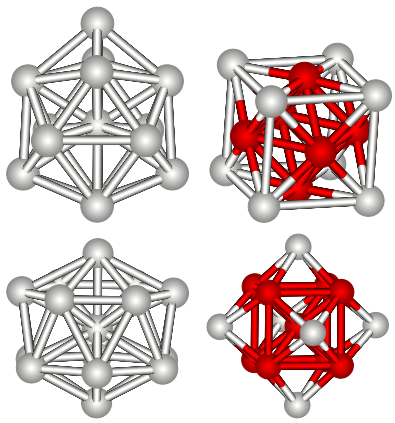

Figure 6: Transitions from Frank-Kasper polyhedra to fcc (first row; $N = 14$, $z_A^*/z_B^* \geq 2.2$) or bcc (second row, $N = 15$, $1.4 \leq z_A^*/z_B^* \leq 2.3$) symmetries.

corresponding to the magic pair $\{10, 22\}$, whose structure is presented in Figure 5, has also a fcc symmetry.

Although the icosahedral symmetry is dominant, for small sizes ($N < 20$) many of the ground-state structures obtained for homo-atomic clusters are the so called Frank-Kasper polyhedra.[32, 33] For example, we have obtained Frank-Kasper polyhedra for $N = 8$, 11, 14 and 15, $N = 11$ and $N = 15$ being also magic numbers (although not very pronounced compared to $N = 13$ and $N = 19$ which have icosahedral symmetry).[13] The structures obtained for $N = 14$ and $N = 15$ are presented in the first column of Figure 6. We have found that alloying these clusters with $n_A \geq 2$ usually destroys the symmetry of these structures. For $n_A = 1$, the A atom is placed in the center and the structure remain unchanged. We have found also that for specific concentrations the structures becomes highly symmetric: if 6 atoms from the B_{14} cluster are replaced with specific A atoms such that $z_A^*/z_B^* \geq 2.2$ the ground-state structure become a single fcc cell with the A atoms at the faces of the B-atoms cube; in a similar way, form the B_{15} clusters using A atoms with $1.4 \leq z_A^*/z_B^* \leq 2.3$ we obtain the A_9B_6 cluster whose ground-sate structure has a perfect bcc cell formed by the A atoms while the B atoms find equilibrium positions in the vicinity of the nearest neighbor centers. The ground-state structures of these clusters are presented in Figure 6.

The structures presented in Figure 4 suggest an icosahedral-fcc transition for the A_nB_{38-n} clusters, driven by the variation of concentration (variation of n) at fixed composition (at fixed z_A^*/z_B^* ratio). The 38-atoms binary cluster was previously studied for Co_mPt_{38-m},[9] for mixed rare-gas clusters,[19] Morse binary clusters, [24] and for $Ag-Ni$, $Ag-Cu$, $Pd-Pt$[6, 25, 26] and $Ag-Pd$, $Au-Cu$, $Ag-Au$, $Ag-Pt$, $Pd-Au$[25, 27] nanoparticles using a genetic algorithm approach with Gupta-like potentials locally optimized using DFT, where transitions form fcc to icosahedral symmetries can be identified. This type of transition has been obtained for various cluster sizes, especially at large z_A^*/z_B^* ratio. Our potential favors icosahedral structures for homo-atomic clusters with $N = 38$, a situation which also occurs for Morse clusters, for certain potentials widths.[24] In fact, there is a good agreement between the homo-atomic ground-state structures and magic numbers obtained within the present approach[13] and those obtained using Morse interactions with certain potential parameters.[23] Also, in Refs.[9, 6, 19] the ground-state structures for $N = 38$ homo-atomic clusters exhibit a fcc-symmetry and alloying gives rise to icosahedral core-shell structures. Here, we find an inverted transition, from an icosahedral structure in pure clusters to a fcc-like structure in binary clusters with very dissimilar type of atoms. For atoms with z_A^*/z_B^* close to 1, which seems to be the case for $Co-Pt$ clusters ($z_{Co}^*/z_{Pt}^* \simeq 1.1$), the structures remains icosahedral also for binary clusters. In this respect, our results agree with the structures reported in Ref.[9] (where the structures are icosahedral from $m = 5$ to $m = 35$). A large number of icosahedral structures were obtained also for $Ag-Cu$ and $Ag-Pd$.[26, 27] but the fcc-like structures were also present, especially for $Ag-Pd$. Our estimation for the effective valence charges gives $z_{Pd}^*/z_{Ag}^* \simeq 2$ and $z_{Cu}^*/z_{Ag}^* \simeq 1.4$, values for which we can observe the above mentioned icosahedral-fcc transitions. We may note also that the magic structure $A_{14}B_{24}$ presented in Figure 4 was obtained also for $Pt_{14}Pd_{24}$ as being highly stable.[27] We have obtained that this structure is groundstate for $1.3 \leq z_A^*/z_B^* \leq 2.2$ and our estimation for $z_{Pt}^*/z_{Pd}^* \simeq 1.3$ is in this range. On the other hand, this ratio is slightly outside the range $1.4 - 2.0$ for which the pair {14,24} is magic according to our definition. We may also note that perhaps a better agreement between our structures and those presented in Refs. [26, 27] is found for the 34-atoms clusters, especially for $Ag-Cu$ and $Ag-Ni$ where the icosahedral structures (fivefold pancake) are predominant.

A new kind of structural transition, a composition induced transition, is obtained for fixed numbers of atoms A and B (fixed concentration), by varying z_A^*/z_B^*, *i.e.* by replacing at least one type of atom with one having a different effective charge. For example, the cluster $A_{14}B_{24}$ has two structural transitions, its ground-state being of icosahedral type (slightly disordered) for $z_A^*/z_B^* \leq 1.2$, fcc for $1.3 \leq z_A^*/z_B^* \leq 2.2$ and icosahedral for

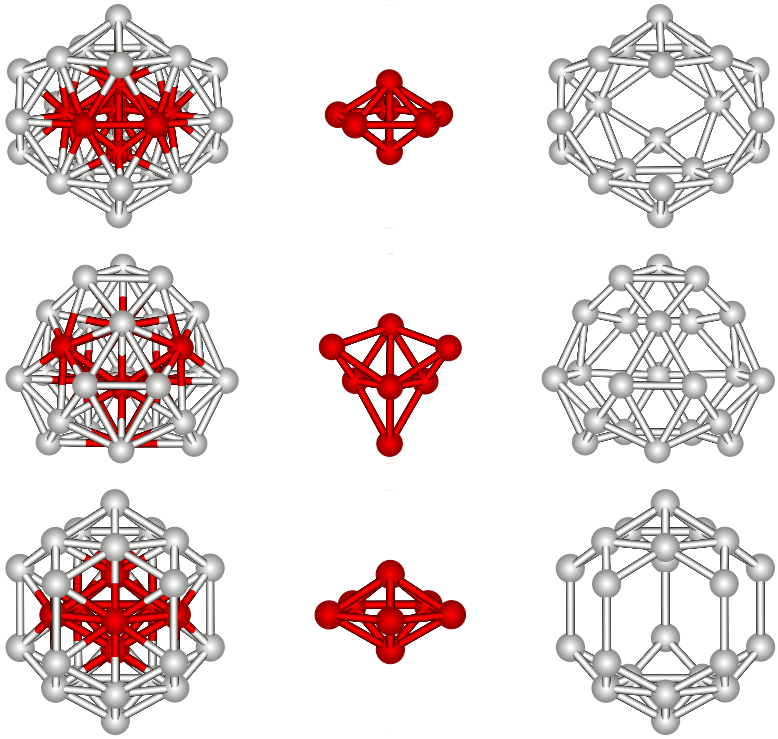

Figure 7: Structural transitions in the A_7B_{22} cluster. The top row represents the ground state for $z_A^*/z_B^* \leq 1.5$, the middle row corresponds to $1.6 \leq z_A^*/z_B^* \leq 1.9$ and the bottom row to $z_A^*/z_B^* \geq 2.0$.

$z_A^*/z_B^* \geq 2.3$. The existence of these structural domains bounded by structural transition points is a general feature of binary clusters. It is not restricted to magic pairs; moreover, it has been obtained for almost all combinations (compositions) A_nB_m. Because we have performed our study with step 0.1 of the parameter z_A^*/z_B^* we can identify with this accuracy the location of the transition points. For instance, in the above example, we have two transition points, one located between $1.2 - 1.3$ and another between $2.2 - 2.3$. Often, for the left-right values which border the transition points we can observe ground-state$\longleftrightarrow$isomer inversions, *i.e.* the left ground-state becomes the right isomer and (or) the left isomer becomes the right ground-state. This implies that, at the transition points, the ground state is degenerate; we have two structures with different symmetries but with the same cohesion energy. Of course, there remains the question of finding two atomic species whose effective valence ratio has this critical value. On the other hand, even if we find such atomic species, it is likely that quantum corrections to the quasi-classical description[13] remove this degeneracy. In this respect, the correct conclusion is that it is possibly to synthesize binary metallic clusters, made up of specific atoms, with very small gaps between the ground-state and the first isomers. These small gaps could imply an increased experimental abundance even if they are not magic (the theoretical abundance spectrum is referred to the ground-state structures; the existence of such small gaps for specific compositions could locally alter this spectrum). On the other hand the task of producing clusters with a specific geometry will become difficult in the presence of this shape degeneracy.

Another example of a composition-induced structural transition is the cluster A_7B_{22}. As we can see in Figure 7 we have obtained three equilibrium structures for various compositions. When we vary the ratio z_A^*/z_B^* the structure presented in the top row of Figure 7 remains ground-state for $z_A^*/z_B^* \leq 1.5$ and becomes the first isomer for $z_A^*/z_B^* = 1.6$. We have a transition point somewhere between $z_A^*/z_B^* = 1.5$ and $z_A^*/z_B^* = 1.6$. The structure presented in the middle row of Figure 7 is found to be the ground-state for $1.6 \leq z_A^*/z_B^* \leq 1.9$ and the first isomer for $z_A^*/z_B^* = 2.0$. We have here a second transition point. The structure of the first isomer for $z_A^*/z_B^* = 1.9$, presented in the bottom row of Figure 7 becomes ground state for $z_A^*/z_B^* \geq 2.0$. Although very common, this inversion between the ground-state and the first isomer in the vicinity of a transition point cannot be generalized as a rule. For example, at the first transition point for the cluster A_7B_{22} we have inversion only in one way: the ground-state for $z_A^*/z_B^* = 1.5$ becomes isomer for $z_A^*/z_B^* = 1.6$ but the first isomer for $z_A^*/z_B^* = 1.5$ and the ground-state for $z_A^*/z_B^* = 1.6$ do not have the same structure. They do have similar core structure but the outside shells are equilibrated in slightly different configurations.

We may note also that the structure presented in the last row in Figure 7 has a star-shaped appearance when viewed from above as in Figure 8 and has been previously obtained using the many-body Gupta potential for the 29-atom $Pd - Pt$ cluster at various concentrations.[10, 11]

Beside the core-shell segregation, which is dominant for binary nano-clusters, we can identify another type

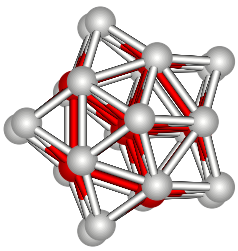

Figure 8: The star-shaped ground-state of the cluster A_7B_{22} for $z_A^*/z_B^* \geq 2$.

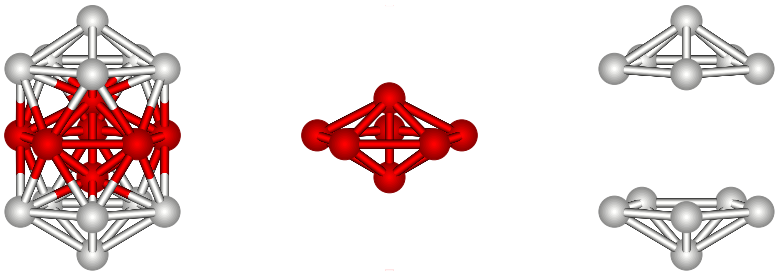

Figure 9: The domain walls segregation in the cluster A_7B_{12} irrespective of the ratio z_A^*/z_B^*.

of segregation. In the structure shown in the bottom row in Figure 7 the B-atoms occupy two distinct regions (up-down) separated by an A-atoms region. This kind of domains walls segregation is very rare, the core-shell segregation being predominant; it has been obtained also for the cluster A_7B_{12}, whose structure is presented in Figure 9. A similar segregation has been obtained for the Lennard-Jones cluster A_7B_{12}[2] and also in $Co-Pd$ nanoclusters for sizes $N = 13$ and $N = 19$, using a genetic algorithm in combination with a Gupta potential. On the other hand the segregation shown in Figure 9 can be described as a surface segregation, because the 12 B atoms, instead of forming a uniform closed surface around the 7 atoms A-core, segregate in two distinct regions diametrically opposite on that surface. Moreover, a surface segregation can be observed also in the structure of the cluster $A_{26}B_{12}$ shown in Figure 4. There, the 12 B atoms forming the outside shell segregate in 4 distinct regions, each region consisting of 3 B atoms closely bound together. Such a surface segregation could be interpreted as a variable surface composition in experimental measurements. Evidence for a variable surface composition in Ar/Xe clusters in photoelectron spectroscopy has been reported in Ref. [29].

Varying the ratio z_A^*/z_B^* we can obtain all the possible structures for a specific nanoalloy, which can be used as an input for *ab initio* calculations. The values of the effective valence charges z^* can be viewed as input parameters in the present theoretical model. Exploring a large domain for the values of these effective charges we have obtained qualitative results like segregation or structural transitions driven by concentration or composition in good agreement with other models. In order to compare numerical values, as binding energies or interatomic distances, we can use as a first approximation the estimation[13] $z^* = z(1+0.84Z^{1/3})\exp(-0.84Z^{1/3})$, where z is the nominal valence and Z is the atomic number. It is customary to use the 13-atom clusters as a benchmark against *ab initio* DFT calculations. In Table 1 we pressent such a comparation with other high-level calculations for Co ($Z = 27$, $z = 2$, $z^* = 0.566$), Pt ($Z = 78$, $z = 4$, $z^* = 0.507$) and Cu ($Z = 29$, $z = 1$, $z^* = 0.271$) metallic clusters. In all cases the icosahedral structure is the ground-state structure; as we can see in Table 1 there is a good agreement for binding energies and interatomic distances. The same level of agreement is maintained for binary 13-atom clusters. We obtained for example a binding energy of 2.93eV per atom for Co_6Cu_7 which is very close to the value 3.08eV per atom obtained in Ref. [35] by a DFT optimization of the structures resulted from a genetic algorithm with a Gupta-like many-body potential. Similarly, we obtain a binding energy of 4.8eV per atom for $Co_{12}Cu$, which compares well with the values $4.15-4.23$eV per atom from Ref. [35]. For Cu-rich clusters the agreement is poorer; the same behavior can be observed in pure Cu clusters, although the interatomic distances are in good agreement. We can suspect here a poor estimation of the effective charge. We have compared also the binding energies per atom for $Co-Pt$ clusters. For example, we obtained 4.14eV, 4.55eV and 5.04eV for $CoPt_{12}$, Co_6Pt_7 and $Co_{12}Pt$, which compare well with the values 3.49eV, 3.66eV and 4.45eV taken from Ref. [35]

For $Co-Pd$ clusters ($Z_{Pd} = 46$, $z_{Pd} = 2$, $z_{Pd}^* = 0.395$) we have compared our results with those obtained in Ref. [12] for N =7, 13, 19, 23 and 26 using a Gupta potential in combination with a genetic algorithm energy minimization and checked with DFT calculations for some selected clusters. Al the structures reported there are in agreement with our calculations. We have obtained decahedral structures for $N = 7$ and simple, double, triple and, respectively, quadruple icosahedral structures for $N = 13$, 19, 23 and 26. The Co atoms, with higher effective charges ($z_{Co}^* = 0.566$), tends to segregate at the center forming, for example, a tetrahedron in

	z^*	E/N(eV)	L_b(Å)	Refs.
	0.566	5.12	2.00	
Co_{13}		4.89	2.42	Ref. [9]
		4.08	2.33	Ref. [34]
		4.48	2.49	Ref. [35]
	0.507	4.06	2.08	
Pt_{13}		3.47	2.79	Ref. [35]
		4.38	2.79	Ref. [9]
		4.43	2.6	Ref. [36]
Cu_{13}	0.271	1.12	2.56	
		2.19	2.55	Ref. [35]

Table 1: Binding energies per atom and the first nearest distance for various metallic clusters compared with other results.

Co_4Pd_{22}, a hexahedron (triangular bipyramid) in Co_5Pd_{21} or a capped hexahedron in Co_6Pd_{20}. If the number of Pd atoms is insufficient to form an outside shell (large Co concentrations) we can identify mixed outside $Co-Pd$ shells or domain wall segregation like in Figure 9. Nevertheless, the general trend remain the core-shell icosahedral segregation. The interatomic distances are also in good agreement with those obtained in Ref. [12]. For example, we have obtained a $Co-Co$ distance of 2.62Å (compared to 2.39Å), the mean nearest neighbor $Co-Pd$ distance 2.36Å (compared with 2.44Å) and $Pd-Pd$ distance 2.31Å (compared with 2.50Å) for the Co_2Pd_5 cluster. Another example is Co_7Pd_{12}; we obtained the mean nearest-neighbor distances: 2.07Å for $Co-Co$ (compared with 2.34Å), 2.06Å for $Co-Pd$ (compared with 2.52Å) and 2.22Å for $Pd-Pd$ (compared with 2.62Å).

It is worth emphasizing that there are also differences between our results and other numerical calculations. Some of them are a consequence of the form of the potential, like the already mentioned preference for icosahedral structures in homo-atomic clusters. (We can note here that sometime there is no consensus regarding the lowest energy structures for more simple compounds like, for example, Pt_{13} (see for instance Ref. [10])). Other differences could arise from our poor estimation of the effective valence charges, and the point-like approximation. That could be the case for the star-shaped structure from Figure 9 obtained as a ground-state for $z_A^*/z_B^* \geq 2$. This shape was also obtained for $Pd-Pt$ clusters in Ref. [10], but our estimation gives $z_{Pt}^*/z_{Pd}^* \simeq 1.3$.

4 Conclusions

In conclusion, despite the relatively small cluster sizes, we have obtained the general characteristics of binary metallic clusters: the magic pairs in the stability spectra, the radial, domain walls and surface segregation, the new ground-state geometries with fcc symmetry and the structural transitions induced by change in composition or concentration. Two types of transitions have been identified: one by varying the ratio z_A^*/z_B^* and another by varying the relative concentration for a fixed ratio z_A^*/z_B^*. These features, obtained here for bimetallic clusters consisting of up to 40 atoms, are expected to hold also for larger binary clusters although new structures and segregation types could appear, like, for example magic icosahedrons with alternating shells[37] or patchy multi-shell chemical ordering.[38] It is worth noting that by adding an interaction energy with a metallic surface[15] to the quasi-classical energy given by (2), the present approach can be applied to binary metallic clusters deposited on surfaces, which is the common environment for most of the intended technical applications. In addition, despite the increase in the number of isomers which requires even larger statistics there are no impediments in applying this method to trimetallic clusters or more complex hetero-metallic clusters.

Acknowledgments

The author is indebted to M. Apostol for useful discussions. This work was partially supported by Contract Nos CEx05-D11-67 and PN-09-37-01-02 of the Romanian Ministry of Education and Research.

References

[1] R. Ferrando, J. Jellinek and R. Johnston, *Chem. Rev.* **2008**, 108, 845-910.

[2] J. P. K. Doye and L. Meyer, *Phys. Rev. Lett.* **2005**, 95, 063401; arXiv:cond-mat/0604250.

[3] R. P. Gupta, *Phys. Rev. B* **1981**, 23, 6265-6270.

[4] V. Rosato, M. Guillope and B. Legrand, *Philos. Mag. A* **1989**, 59, 321-336.

[5] A. P. Sutton and J. Chen, *Philos. Mag. Lett.* **1990**, 61, 139-146.

[6] G. Rossi, A. Rapallo, C. Mottet, A. Fortunelli, F. Baletto, and R. Ferrando, *Phys. Rev. Lett.* **2004**, 93, 105503.

[7] R. Ferrando, A. Fortunelli and G. Rossi, *Phys. Rev. B* **2005**, 72, 085449.

[8] G. Barcaro, A. Fortunelli, G. Rossi, F. Nita and R. Ferrando, *J. Phys. Chem. B* **2006**, 110, 23197-23203.

[9] Q. L. Lu, L. Z. Zhu, L. Ma and G.H. Wang, *Phys. Lett. A* **2006**, 350, 258-262.

[10] C. Massen, T. V. Mortimer-Jones and R. L. Johnston, *J. Chem. Soc., Dalton Trans.* **2002**, 4375-4388.

[11] L. D. Lloyd, R. L. Johnston, S. Salhi and N. T. Wilson, *J. Mater. Chem.* **2004**, 14, 1691-1704.

[12] F. Aguilera-Granja, A. Vega, José Rogan, X. Andrade and G. García, *Phys. Rev. B* **2006**, 74, 224405.

[13] L. C. Cune and M. Apostol, *Phys. Lett. A* **2000**, 273, 117-124.

[14] L. C. Cune and M. Apostol, *Dig. J. Nano. Bio.* **2007**, 2, 315-333.

[15] L. C. Cune and M. Apostol, in *Low-Dimensional Systems: Theory, Preparation, and Some Applications*, 1-17, eds. Luis M. Liz-Marzan et al., Kluwer Academic Publisher, **2003**.

[16] L. C. Cune and M. Apostol, *Chem. Phys. Lett.* **2001**, 344, 287-291.

[17] R. Smoluchowski, *Phys. Rev.* **1941**, 60, 661-674.

[18] A. A. Frost and B. Muslin, *J. Chem. Phys.* **1954**, 22, 1017-1020.

[19] F. Calvo and E. Yurtsever, *Phys. Rev. B* **2004**, 70, 045423.

[20] W. A. de Heer, *Rev. Mod. Phys.* **1993**, 65, 611-676.

[21] M. Brack, *Rev. Mod. Phys.* **1993**, 65, 677-732.

[22] F. Baletto and R. Ferrando, *Rev. Mod. Phys.* **2005**, 77, 371-423.

[23] J. P. K. Doye and D. J. Wales, *J. Chem. Soc. Faraday Trans.* **1993**, 93, 4233-4243.

[24] D. Parodi and R. Ferrando, *Phys. Lett. A* **2007**, 367, 215-219.

[25] L. O. Paz-Borbón, R. L. Johnston, G. Barcaro and A. Fortunelli, *J. Chem. Phys.* **2008**, 128, 134517.

[26] A. Rapallo, G. Rossi, R. Ferrando, A. Fortunelli, B. C. Curley, L. D. Lloyd, G. M. Trabuck and R. L. Johnston, *J. Chem. Phys.* **2005**, 122, 194308.

[27] G. Rossi, R. Ferrando, A. Rapallo, A. Fortunelli, B. C. Curley, L. D. Lloyd and R. L. Johnston, *J. Chem. Phys.* **2005**, 122, 194309.

[28] M. Gaudry, E. Cottancin, M. Pellarin, J. Lermé, L. Arnaud, J. R. Huntzinger, J. L. Vialle, and M. Broyer, *Phys. Rev. B* **2003**, 67, 155409.

[29] M. Tchaplyguine, M. Lundwall, M. Gisselbrecht, G. Öhrwall, R. Feifel, S. Sorensen, S. Svensson, N. Mårtensson and O. Björneholm, *Phys. Rev. A* **2005**, 69, 031201(R).

[30] M. Cazayous, C. Langlois, T. Oikawa, C. Ricolleau, and A. Sacuto, *Phys. Rev. B* **2006**, 73, 113402.

[31] F. Calvo, E. Cottancin and M. Broyer, *Phys. Rev. B* **2008**, 77, 121406(R).

[32] F. C. Frank and J. S. Kasper, *Acta. Cryst.* **1958**, 11, 184-190.

[33] F. C. Frank and J. S. Kasper, *Acta. Cryst.* **1959**, 12, 483-499.

[34] H. M. Duan, Q. Q. Zheng, *Phys. Lett. A* **2001**, 280, 333.

[35] Q. L. Lu, L. Z. Zhu, L. Ma and G. H. Wang, *Chem. Phys. Lett.* **2005**, 407, 176-179.

[36] A. Sebetei, Z. B. Guvenc, Surf. Sci. **2003**, 525, 66-84.

[37] P. Entel and M. E. Gruner, *J. Phys.: Condens. Matter* **2009**, 21, 064228.

[38] G. Barcaro, A. Fortunelli, M. Polak and L. Rubinovich, NanoLett. 2011, 11, 1766-1769.